THE APPLICATION OF ELECTROMAGNETIC THEORY TO ELECTROCARDIOLOGY

II. Numerical Solution of the Integral Equations

A. C. L. BARNARD, I. M. DUCK, M. S. LYNN, *and* W. P. TIMLAKE

From the IBM Scientific Center, Houston, Texas 77025

ABSTRACT In an earlier paper exact integral equations were derived for the surface potentials resulting from sources within an irregularly shaped inhomogeneous body. These exact equations cannot usually be solved. In this paper a discrete analogue is constructed which is not straightforward to solve, but which can be treated by careful mathematical methods. In particular a deflation procedure greatly facilitates the iterative solution of the problem and overcomes the divergence encountered by other authors. Numerical solutions obtained for simple geometries are compared to the exact analytic solutions available in such cases. The necessary convergence of the solutions of the discrete analog towards the solution of the continuous problem is shown to occur only if the coefficients of the discrete analogue are carefully evaluated. Calculations are then presented for realistic thoracic geometries, typical results being presented as surface potential maps. Finally the important effect of the internal regional inhomogeneities, particularly a realistic cardiac blood mass, is demonstrated by obtaining vector loops with and without these effects.

I. INTRODUCTION

In the preceding paper (1), which will be referred to as I, integral equations were rigorously derived for the surface potentials resulting from a source in an irregularly shaped body. The body was considered to consist of various regions, each internally homogeneous, but with electrical properties varying from one region to another. Thus, the torso could be modeled by a basic air-surrounded volume containing within it regions to represent the lungs, the blood masses in the ventricles, and so on. Equations including the time-dependent effects were given in I, but only the steady-state equations will be considered here, i.e., all time derivatives will be set to zero in the equations in I.

It will be recalled from I that there are two ways of formulating the problem. One way (related to the method used by Gelernter and Swihart (8–10), is to construct an integral equation for the charge densities on all surfaces. If the solution to this equa-

tion is known, the potential at any point on the surface is then obtained from Coulomb's law. The second, known as the "direct method," (used by Barr et al., 2) is to construct an integral equation for the potential at any point on the surface (13). In either case the original continuous integral equation cannot usually be solved and must be replaced by a "discrete analogue," which is a linear system of algebraic equations whose solutions can be found. In this paper we discuss the construction and solution of the discrete analogue. Other authors (2, 8–10) have, of course, used such analogues, but the equations are quite subtle to treat since, as shown in section II, the system obtained is in principle *singular.* (In practice the system may not be quite singular because of the use of numerical approximations, but will be extremely ill-conditioned.) The singularity of the exact coefficient matrix may not have been noted by the authors (2, 19) who suggest directly inverting this matrix. If the inverse exists, it is only because of numerical errors. To our knowledge, however, no workers have tried to use this method since the order of the matrices involved is usually large. Thus, an iteration procedure is used which, as Plonsey (19) says, "hopefully converges to the correct distribution." However, the near-singularity of the system has introduced difficulties in proposed iteration procedures, and convergence is by no means guaranteed. Hints in the literature (20) and personal communications indicate that various workers have met the problem of iterative divergence. We shall demonstrate divergence at several points of this paper, but, of course, our main objective is to *show how to avoid it by using properly constructed algorithms to solve the problem* (section II).

Thus, the first requirement on the discrete analogue is that it can be solved reliably using adequate algorithms. A second requirement is that the discrete analogue must be the "same" problem as the original continuous problem, in the sense that as the dimensions of the matrices increase towards infinity, the solutions of the discrete analogue tend to those of the continuous problem. It will be demonstrated theoretically (section III) and numerically (section V) that this is the case for the methods proposed in this paper. Some methods used by other authors (2, 8–10), do not have this essential property.

After adequate numerical procedures have been developed, they will be applied in section VI to a realistic torso model, and calculated surface potential maps will be shown. For the first time the full effects of realistic cardiac ventricular blood masses, as well as the pulmonary volumes, are included.[1] Some results concerning the effects of the pulmonary volumes alone have been announced in reference 14.

Finally, in section VII we consider briefly a simple case of the inverse problem, in order to emphasize that the modeling assumptions of the thorax are certainly significant.

---

[1] A preliminary announcement of this was made at the SIAM National Meeting, University of Iowa, May, 1966 (16).

The mathematics outlined in this paper may, perhaps, appear somewhat complicated for a biological problem. Unfortunately, the numerical problems encountered in this application are sufficiently subtle to demand such a discussion as a minimum. The equations arising in this problem are not special to electrophysiology, but arise in a large variety of applications. In other contexts other authors have attacked this problem numerically (see reference 17 for a fuller discussion and bibliography).

II. THE DISCRETE ANALOG

The problem of interest in electrocardiology is the multi-interface problem (1, 2, 8–10, 14, 19). A full mathematical analysis of this general problem is complex and beyond the scope of this paper (although we shall give some numerical results in later sections). Thus, we shall confine our attention for the most part to a careful discussion of the single interface problem, i.e., a homogeneous volume V, bounded by a closed surface S. A full discussion of the theory of the multiple-interface problem is given elsewhere (18).

A. *Properties of the Integral Equations*

In I it was shown that the surface density of "total" charge, W at a point $\mathbf{r}$ on the surface S, satisfied the integral equation

$$W(\mathbf{r}) = -\frac{\partial}{\partial \mathbf{n}_r}\Phi_m(\mathbf{r}) + \int_S K(\mathbf{r}, \mathbf{r}')W(\mathbf{r}')\,dS' \tag{1}$$

(equation 50 of I) when $\mathbf{n}_r$ is the normal direction at $\mathbf{r}$, Φ_m is the known potential that would be produced by the given sources in an infinite medium, and the kernel is given by

$$K(\mathbf{r}, \mathbf{r}') = (-\tfrac{1}{2}\pi)(\partial/\partial \mathbf{n}_r)(1/|\,\mathbf{r} - \mathbf{r}'\,|). \tag{2}$$

The potential is then computed from W by evaluating the Coulomb's law integral

$$\Phi(\mathbf{r}) = \Phi_m(\mathbf{r}) + \left(\frac{1}{2\pi}\right)\int [W(\mathbf{r}')/|\,\mathbf{r} - \mathbf{r}'\,|]\,dS' \tag{3}$$

which was equation 51 of I.

An alternate approach (1, 2) is to obtain Φ directly as the solution of the integral equation

$$\Phi(\mathbf{r}) = 2\Phi_m(\mathbf{r}) + \int_S K(\mathbf{r}', \mathbf{r})\Phi(\mathbf{r}')\,dS' \tag{4}$$

(equation 61 of I), and we note that the kernel in equation 4 is the transpose of that

in equation 1. In order to establish a sound numerical algorithm, we must first consider some properties of the exact integral equations 1 and 4.

The "transposed homogeneous equation" (5) is obtained by setting $\Phi_m \equiv 0$ in equation 4. It is easy to show that Φ = constant is the only nontrivial solution of this equation (physically this corresponds to the arbitrary constant which can be added to potentials.). But according to the extension (p. 309 of reference 13) of a basic theorem of linear integral equations (the "Fredholm Alternative") (5, 13), if the transposed homogeneous equation has nontrivial solutions χ, the inhomogeneous equation 1 has solutions if and only if

$$\int_S f(\mathbf{r})\chi(\mathbf{r})\, dS = 0 \tag{5}$$

where

$$f(\mathbf{r}) = (-\partial/\partial \mathbf{n}_r)\Phi_m(\mathbf{r}) \tag{6}$$

is the inhomogeneous part of equation 1. Physically, however, with particular χ and f that we have, equation 5 is just Gauss's law in electrostatics and is thus satisfied for any source with no net charge (dipoles, quadrupoles, etc.). Thus, solutions to equation 1 exist, and solutions to its transpose, equation 4, also exist. The solutions, however, are not unique. Since $\Phi \equiv$ constant is the only solution to the transposed homogeneous equation, solutions of equations 1 or 4 may be made unique by imposing some additional condition such as

$$\int_S W(\mathbf{r})\, dS = 0. \tag{7}$$

Although we know that solutions to the exact integral equations 1 and 4 exist, we do not know how to find them; in fact, exact analytic solutions can only be found in special cases, for example when the surfaces are spheres (24) or prolate spheroids (3). For the convoluted surfaces involved in electrocardiology we have to define numerical algorithms to obtain the approximate solutions. We now turn our attention to this.

B. *Matrix Form of the Equations*

We divide the surface S up into elements Δ_i $(i = 1 \cdots n)$. In practice these area elements will have a small "diameter." Define

$$\omega_i = \int_{\Delta_i} W\, dS \tag{8}$$

and

$$f_i = \int_{\Delta_i} f\, dS. \tag{9}$$

Then integrating equation 1 over Δ_i, we obtain

$$\omega_i = f_i + \int_{\Delta_i} \left[\int_S K(\mathbf{r}, \mathbf{r}') W(\mathbf{r}')\, dS \right] dS_i. \tag{10}$$

In the last integral the order of integration may be interchanged and the result written in terms of integrals over the elements:

$$\int_S \left[\int_{\Delta_i} K(\mathbf{r}, \mathbf{r}')\, dS_i \right] W(\mathbf{r}')\, dS' = \sum_{j=1}^{n} \int_{\Delta_j} \left[\int_{\Delta_i} K(\mathbf{r}, \mathbf{r}')\, dS_i \right] W(\mathbf{r}')\, dS_j'. \tag{11}$$

The integral over Δ_i is just $\Omega_{\Delta_i}(\mathbf{r}')$, the solid angle (in units of 2π) subtended by the ith surface element at this point $\mathbf{r}'$. Thus,

$$\omega_i = f_i + \sum_j \int_{\Delta_j} \Omega_{\Delta_i}(\mathbf{r}') W(\mathbf{r}')\, dS_j'. \tag{12}$$

We now use the following identity for integrable functions Ω and W:

$$\mu_j^2 \int_{\Delta_j} \Omega(\mathbf{r}') W(\mathbf{r}')\, dS' \equiv \mu_j \int_{\Delta_j} \Omega(\mathbf{r}')\, dS' \int_{\Delta_j} W(\mathbf{r}'')\, dS'' + \zeta_j(W, \Omega), \tag{13}$$

where

$$\zeta_j(W, \Omega) = \iiint_{\Delta_j} [\mathbf{W}(\mathbf{r}') - W(\mathbf{r}'')][\Omega(\mathbf{r}') - \Omega(\mathbf{r})]\, dS\, dS'\, dS'' \tag{14}$$

and μ_j is the area of the element Δ_j. The basic idea is that the term $\zeta(W, \Omega)$ is expected to be "small" since the functions are continuous and the surface elements are "small." This point will be considered further in section III. Then

$$\omega_i = f_i + \sum_j b_{ij}\omega_j + \zeta_i[W] \tag{15}$$

where

$$b_{ij} = \mu_j^{-1} \int_{\Delta_j} \Omega_{\Delta_i}(\mathbf{r}')\, dS_j' \tag{16}$$

and

$$\zeta_i[W] = \sum_{j=1}^{n} \zeta_j(W, \Omega_{\Delta_i}). \tag{17}$$

We have used the notation $\zeta[W]$ to emphasize that ζ depends on the unknown solution W; clearly it also depends upon Ω_{Δ_i}, but we omit this dependence for clarity.

Thus, b_{ij} is the solid angle subtended by the ith element at the jth element, aver-

aged over points on the jth element. An equation like 15 exists for each element, i.e., $i = 1, 2, \cdots, n$. The set may be written as a single matrix equation

$$(\mathbf{I} - \mathbf{B})\omega = \mathbf{f} + \zeta[W] = \mathbf{F}[W]. \tag{18}$$

The integral equation for potential, equation 4, may be treated in a similar way. Let

$$\varphi_i = \mu_i^{-1} \int_{\Delta_i} \Phi \, dS \tag{19}$$

and

$$g_i = \mu_i^{-1} \int_{\Delta_i} 2\Phi_m \, dS. \tag{20}$$

Then

$$(\mathbf{I} - \mathbf{B}^*)\varphi = \mathbf{g} + \xi[\Phi] = \mathbf{G}[\Phi] \tag{21}$$

where here and below the asterisk denotes the transpose matrix $b_{ij} \rightarrow b_{ji}$. The term $\xi[\Phi]$ is analagous to $\zeta[W]$ in equation 18.

It can be similarly shown from equation 3 that the expression giving potential once charge is known is

$$\varphi - \mathbf{R}\omega = \mathbf{g} + \mathfrak{n}[W] = \mathbf{H}[W] \tag{22}$$

where

$$R_{ij} = \mu_i^{-1}\mu_j^{-1} \int_{\Delta_i} \int_{\Delta_j} [1/|\mathbf{r} - \mathbf{r}'|] \, dS \, dS' \tag{23}$$

and $\mathfrak{n}[W]$ is analogous to ζ and ξ. Note that equations 12, 13, and 22 are still exact. That is they hold for the solutions of the continuous equations 1 and 4, and we have made no discrete approximations. For example, the union of all the surface elements Δ_i exactly forms the surface S.

C. *Difficulties in Solving the Matrix Equations*

Solutions to equations 18 and 21 certainly exist, since solutions to equations 1 and 4 exist. However, we still do not have a solvable problem, since ζ, ξ, and $\mathfrak{n}$ depend on the unknown function W and Φ. Further, we cannot evaluate **B**, **f**, and **g** precisely for the "exact" surface elements. Thus, there are three questions to be resolved:

(*a*) *Is it legitimate to construct an algorithm by assuming* ζ, ξ, *and* $\mathfrak{n}$ *small and omitting them in equations 18, 21, and 22?* Assuming we had approximations to **B**,

f, and g, we should then have a system of n linear algebraic equations in n unknowns. (*b*) *What will be the effect of numerically approximating the quantities* **B**, **f**, *and* **g**? (*c*) *Assuming* (*a*) *and* (*b*) *are resolved, how should the resultant system of n linear algebraic equations be solved when n is large?* This latter point will be discussed in section IV.

In order to consider point (*a*) we need to establish a property of matrix **B** and use some results from linear algebra.

First note that from equation 16

$$\sum_{i=1}^{n} b_{ij} = \mu_j^{-1} \int_{\Delta_j} \left(\sum_i \Omega_{\Delta_i}\right) dS' = \mu_j^{-1} \int_{\Delta_j} \Omega_B \, dS' = 1$$

since the solid angle in units of 2π subtended by a closed surface at a point of itself is unity. In matrix notation

$$\mathbf{e}^*\mathbf{B} = \mathbf{e}^* \text{ (equivalently } \mathbf{B}^*\mathbf{e} = \mathbf{e}) \tag{24}$$

where $\mathbf{e}^*$ is a row vector with all unit entries, that is **B** has an eigenvalue, λ, at $\lambda = 1$. We shall assume (17) that this eigenvalue is "simple," so that scalar multiples of $\mathbf{e}^*$ are the *only* vectors satisfying equation 24. Thus, $(\mathbf{I} - \mathbf{B})$, where **I** is the identity matrix, has a simple eigenvalue at 0, i.e., $(\mathbf{I} - \mathbf{B})$ is singular. Thus, solutions to equations of form

$$\mathbf{q} = \mathbf{B}\mathbf{q} + \mathbf{h} \tag{25}$$

do not necessarily exist. The necessary and sufficient condition that they exist is $\mathbf{e}^*\mathbf{h} = 0$. [We have been making use of theorems in linear algebra (5) which parallel the Fredholm alternative: $\mathbf{e}^*$ is the nontrivial solution to the transposed homogeneous equation, and the existence condition is similar to equation 5.]

Since **B** has a "left eigenvector" $\mathbf{e}^*$ (equation 24), it must also have a "right eigenvector" **x**

$$\mathbf{B}\mathbf{x} = \mathbf{x} \text{ (equivalently } \mathbf{x}^*\mathbf{B}^* = \mathbf{x}^*), \tag{26}$$

and if $\mathbf{B}^*$ replaced **B** in equation 25, the condition for existence of solutions would be $\mathbf{x}^*\mathbf{h} = 0$. However, this right eigenvector, **x**, is unknown a priori, unlike the left eigenvector **e**.

Solutions to equations 1 and 4 and hence to equations 18 and 21 exist, so we must have $\mathbf{e}^*\mathbf{F} = \mathbf{x}^*\mathbf{G} = 0$ as can be seen by multiplying equation 18 on the left by $\mathbf{e}^*$ and equation 21 on the left by $\mathbf{x}^*$. However, if we drop ζ and ξ, solutions to the modified equations exist only if

$$\mathbf{e}^*\mathbf{f} = 0 \tag{27}$$

for equation 18 and

$$\mathbf{x}^*\mathbf{g} = 0 \tag{28}$$

for equation 21. Now, as noted below equation 5, $\mathbf{f}$ is the quantity appearing in Gauss's law in electrostatics, so that condition 27 is precisely satisfied for the case of interest. Thus, we may drop ζ from equation 18 without jeopardizing the existence of the solutions:

$$\omega = \mathbf{B}\omega + \mathbf{f}. \tag{18 a}$$

Equation 18 *a* represents a set of linear algebraic equations whose solutions exist. However, condition 28 is *not* necessarily satisfied; if we drop the "small" term from the singular equation 21, the discrete equation

$$\varphi = \mathbf{B}^*\varphi + \mathbf{g} \tag{21 a}$$

probably has no solutions.

Thus, it is out of the question simply to drop the "small" term ξ. One must approach this problem with caution; we shall resolve this later.

We now turn to the point (*b*) above, the problem of evaluating $\mathbf{B}$, $\mathbf{f}$, and $\mathbf{g}$. Although these quantities are precisely *defined*, we cannot *evaluate* them with absolute precision, and we inevitably approximate them by quantities $\hat{\mathbf{B}}$, $\hat{\mathbf{f}}$, and $\hat{\mathbf{g}}$. Gelernter and Swihart (8–10) approximated the b_{ij} by applying the "centroid rule" twice in equation 16:

$$\hat{b}_{ij} = \mu_i(\mathbf{n}_i \cdot \mathbf{r})/r^3 \tag{29}$$

where $\mathbf{n}_i$ is the unit normal vector at the surface element i (area μ_i) and $\mathbf{r}$ is the vector from the centroid of element j to that of element i. This is a poor approximation to b_{ij}, particularly for adjacent surface elements, and can certainly be improved upon. Gelernter and Swihart also approximated f_i by the value of the integrand at the centroid. This is poor for surface elements close to the source. Thus $\mathbf{e}^*\mathbf{f}$ will not be precisely 0, and solutions to the singular equation 18 *a* will not exist. However, because of their approximation to $\mathbf{B}$, Gelernter and Swihart are solving an equation

$$\hat{\omega}_c = \hat{\mathbf{B}}_c\hat{\omega}_c + \hat{\mathbf{f}}_c \tag{30}$$

(where *c* means "centroid rule") which is not necessarily precisely singular. Solutions may exist, but the matrix will be ill-conditioned, and in practice when equation 30 is solved iteratively, instability or divergence will occur except under particularly favorable circumstances (see numerical examples in section VI).

Barr et al. (2) used similar approximations to those above. However, they also adjusted (where necessary) the row sums of $\mathbf{B}^*$ to be exactly unity, thereby ensuring the singularity of $(\mathbf{I} - \mathbf{B}^*)$. Thus, unless $\mathbf{x}^*\mathbf{g}$ is exactly 0, solutions usually do not exist. However, we repeat that the "right eigenvector" $\mathbf{x}$, unlike the left eigenvector $\mathbf{e}^*$, is unknown, and $\mathbf{g}$ cannot be appropriately adjusted.

Even though these difficulties may not manifest themselves in simple cases, such as spheres (the inherent symmetries give favorable properties), we shall show in section V that even in these cases the above approximations are not altogether acceptable. When attempting to solve more complex problems, the difficulties show up dramatically, as will be demonstrated in section VI.

D. *Construction of the Discrete Analogue*

We now develop a scheme for solving the problem, using the above properties to develop an algorithm which is safe, stable, accurate, and convergent.

The first step is to evaluate the b_{ij} more accurately than by the "centroid rule" (equation 29). Observing that the solid angle subtended by a plane triangle at a point can be evaluated analytically (see Appendix I), we choose our surface elements such that they may be well approximated by plane triangles $\hat{\Delta}_i$. At this point we have for the first time approximated our (possibly) curved surface, by a mosaic of plane triangles. Now approximate b_{ij} by

$$\hat{b}_{ij} = \Omega_{\hat{\Delta}_i}(\mathbf{p}) \tag{31}$$

where $\mathbf{p}$ is the centroid of $\hat{\Delta}_j$.[2] Thus

$$\sum_i \hat{b}_{ij} = 1$$

precisely. Equation 31 will be referred to as the "one solid angle" approximation to b_{ij}.

Thus, the column sums of $\hat{\mathbf{B}}$ are unity, apart from the "round-off error" introduced by the finite word-length of the computer. This error is negligible compared to the truncation error of using the "centroid rule." The quantities $\mathbf{f}$ or $\mathbf{g}$ can also be evaluated analytically in part, with similar gains in accuracy. Thus, we take care to retain the singularity of the system. We have shown that at this point it should be possible to solve the discretized charge equation 18 *a* but not the discretized potential equation 21 *a*, since its solutions do not exist. In either case, however, we are still in an unstable situation where small numerical errors can grow and destroy any hope of a meaningful approximation.

Thus, we must proceed somewhat differently, using the concept of deflation. It is mathematically essential to deflate in the case of the potential equation, but it is computationally desirable to deflate the charge equation also, since it makes the computational scheme stable and convergent. The deflation procedure is easy to implement and we now discuss it for a single-surface case. (The multiple-interface deflation is more complex to derive, though simple to implement, and is fully described by Lynn and Timlake, 18.)

[2] Presumably better approximations would involve evaluating the above quantity at several points on the jth triangle and averaging. We have investigated this point briefly.

Let $\mathbf{p}$ be any vector such that

$$\mathbf{p}^*\mathbf{e} = 1.$$

Then it can be shown (4) that

$$\mathbf{C} = \mathbf{B} - \mathbf{p}\mathbf{e}^* \tag{32}$$

has the same eigenvalues as $\mathbf{B}$ except for the one at unity, which is replaced by 0. Thus, since the unit eigenvalue of $\mathbf{B}$ was assumed simple, $(\mathbf{I} - \mathbf{C})$ is nonsingular. Consider the equation

$$\omega = (\mathbf{B} - \mathbf{p}\mathbf{e}^*)\omega + \mathbf{F}. \tag{33}$$

Multiplying from the left by $\mathbf{e}^*$ gives

$$\mathbf{e}^*\omega = (\mathbf{e}^*\mathbf{B} - \mathbf{e}^*\mathbf{p}\mathbf{e}^*)\omega + \mathbf{e}^*\mathbf{F} = \mathbf{e}^*\omega - \mathbf{e}^*\omega + 0,$$

i.e., solutions to equation 33 have the property $\mathbf{e}^*\omega = 0$ and automatically satisfy the physical requirement that the sum of the charges over the surface is 0 (equation 7). This property also ensures that solutions to equation 33 are also solutions to equation 18. Finally, $(\mathbf{I} - \mathbf{B} + \mathbf{p}\mathbf{e}^*)$ in equation 33 is nonsingular, and we can drop ζ without introducing doubts about existence of solutions. For the present let us assume that we can evalute $\mathbf{C}$ exactly. (We return to this point at the end of this section.) Our discrete analogue of equation 18 is therefore

$$(\mathbf{I} - \mathbf{C})\hat{\omega} = \mathbf{f}, \tag{34}$$

i.e., $\hat{\omega}$ is the solution to the discrete analogue. The approximate potential $\hat{\varphi}$ can then be obtained from the discrete approximation to equation 22, i.e.,

$$\hat{\varphi} = \mathbf{R}\hat{\omega} + \mathbf{g}. \tag{35}$$

The treatment of the potential equation is similar. Consider the equation

$$\varphi_p = (\mathbf{B}^* - \mathbf{e}\mathbf{p}^*)\varphi_p + \mathbf{G}[\Phi]. \tag{36}$$

Multiplying equation 36 from the left by $\mathbf{x}^*$ (equation 26) shows that $\mathbf{p}^*\varphi_p = 0$[3] so that the unique solution to equation 36 is that solution to equation 21 for which $\mathbf{p}^*\varphi = 0$. Now the choice of $\mathbf{p}$ was arbitrary except for one condition, and some different vector $\mathbf{q}$ could be chosen, giving solutions φ_q where

$$\varphi_q = (\mathbf{B}^* - \mathbf{e}\mathbf{q}^*)\varphi_q + \mathbf{G}[\Phi]. \tag{37}$$

[3] We have assumed $\mathbf{x}$ normalized: $\mathbf{x}^*\mathbf{e} = 1$.

Subtracting equation 37 from equation 36 gives for the difference $\varphi_p - \varphi_q$ the equation

$$\varphi_p - \varphi_q = \mathbf{B}^*(\varphi_p - \varphi_q) \tag{38}$$

whence the difference must be a multiple of the eigenvector, i.e., from equation 14.

$$\varphi_p - \varphi_q = (\text{constant})\ \mathbf{e} \tag{39}$$

(These are the *only* solutions, assuming **B** has only one eigenvalue at unity.) We therefore see that different choices of the deflation vector **p** correspond to different choices of the "zero of potential." By a similar argument, the solution ω of the charge equation 33 is independent of the choice of the deflation vector **p**.

Since equation 36 is nonsingular, we can omit ξ, and our discrete analogue to equation 21 is

$$(\mathbf{I} - \mathbf{C}^*)\hat{\varphi}_p = \mathbf{g}. \tag{40}$$

Even if we continue to assume that **C** can be evaluated exactly, there is no a priori reason why $\hat{\omega}$ and $\hat{\varphi}_p$ should coincide in the limit as $n \to \infty$ with some solutions ω and φ of the continuous problem. The occurrence of this convergence cannot merely be assumed intuitively but must be established rigorously. In the next section we outline some relevant results from reference 17.

The problem increases in difficulty when one considers that **C**, **f**, and **g** are approximated numerically by $\hat{\mathbf{C}}$, $\hat{\mathbf{f}}$, and $\hat{\mathbf{g}}$. Under certain hypotheses convergence of discrete to continuous can be proved when the "one solid angle" approximation is used, but not when the "centroid rule" is employed. In fact, some of the numerical results in section V will indicate that this convergence is far from assured when the "centroid rule" is used.

III. DISCRETIZATION ERROR BOUNDS

In this section we shall merely quote results from Lynn and Timlake (17) for bounds on the "local" discretization error vectors ζ, $\mathfrak{n}$, and ξ, and the more important "global" error vectors α, β, and β_p defined by

$$\alpha = \omega - \hat{\omega}, \tag{41}$$

$$\beta = \varphi - \hat{\varphi}, \tag{42}$$

$$\beta_p = \varphi_p - \hat{\varphi}_p, \tag{43}$$

where in equation 42 β represents the error involved in computing potential via charge, whereas β_p in equation 43 represents the error involved in calculating the potential φ_p directly.

Our object in quoting these results is to identify the quantities which affect the convergence of the solution of the discrete analogue to those of the original continuous problem.

First we recall that ω_i is the total charge on a surface element whereas φ_i is the average potential. Thus, we use two different measures (norms) of the various errors:

$$S(\zeta) = \sum_{i=1}^{n} |\zeta_i|, \quad M(\mathfrak{n}) = \max_{1 \le i \le n} |\eta_i|, \quad M(\xi) = \max_{1 \le i \le n} |\xi_i|, \quad S(\alpha) = \sum_{i=1}^{n} |\alpha_i|,$$

$$M(\beta) = \max_{1 \le i \le n} |\beta_i|, \quad M(\beta_p) = \max_{1 \le i \le n} |\beta_{p_i}|.$$

Bounds for the local error vectors are:

$$S(\zeta) \le K_1 \delta^{\gamma+1/3} \quad \text{(charge)} \tag{44}$$

$$M(\mathfrak{n}) \le K_1 \delta^{\gamma-1/5} \quad \text{(potential via charge)} \tag{45}$$

$$M(\xi) \le K_1 \delta^{\gamma-1/5} \quad \text{(potential, direct)} \tag{46}$$

where K_1 is some constant, δ is the maximum of the diameters of the surface elements Δ, and γ is a number depending on the curvature of the surface ($0 < \gamma \le 1$).

The following global error vector bounds derive from the additional assumption that S bounds a convex volume:

$$S(\alpha) \le K_1 \delta^{\gamma+1/3}/mn \quad \text{(charge)} \tag{47}$$

$$M(\beta) \le K_1 \delta^{\gamma-2/3}/mn \quad \text{(potential via charge)} \tag{48}$$

$$M(\beta_p) \le K_1 \delta^{\gamma-1/5}/mn \quad \text{(potential, direct).} \tag{49}$$

Here m is the minimum of the b_{ij} for $i \neq j$. *Thus, provided that* (mn) *is bounded away from* 0 *as* $n \to \infty$ *and* $\delta \to 0$, *the discrete solutions converge towards the continuous.*

For a sphere $\gamma = 1$ and $mn \ge \frac{1}{2}$, and thus

$$S(\alpha) \le K_1 \delta^{4/3} \tag{50}$$

$$M(\beta) \le K_1 \delta^{1/3} \tag{51}$$

$$M(\beta_p) \le K_1 \delta^{4/5}. \tag{52}$$

We note that since δ is small, $\delta^{4/5} < \delta^{1/3}$, and for given δ the bounds indicate that the "direct method" should give more accurate potentials than those obtained via the charge equation.

Having given these results, we should add a note of caution on their interpretation:

they are strictly *upper bounds* on the error, and, while it is apparent that this upper bound decreases uniformly as $n \to \infty$, there is no claim that the actual error obtained in any set of calculations will decrease monotonically as $n \to \infty$.

The above results neglected any error in calculating **B**. We now modify the results to take account of the difference. We define

$$\nu = \max_j \sum_{i=1}^{n} | b_{ij} - \hat{b}_{ij} |. \tag{53}$$

Then it can be shown that

$$\nu < \delta^{1/3} \tag{54}$$

where $\hat{\mathbf{B}}$ is calculated by the "one solid angle" rule. The modified results for convex bodies are:

$$S(\alpha) \leq K_1' \text{ max of } [\nu, \delta^{\gamma+1/3}] \leq K_1'\delta^{1/3} \tag{55}$$

$$M(\beta) \leq K_1'\delta^{-2/3} \tag{56}$$

$$M(\beta_p) \leq K_1' \text{ max of } [\nu, \delta^{\gamma-1/5}]. \tag{57}$$

It should be noted that equation 56 indicates divergence, and thus, on the basis of error bounds, it is preferential to compute potential directly rather than via charge. There is some indication of this in practice.

IV. METHOD OF SOLUTION OF EQUATIONS

The linear equations of the discrete analogue (equations 34 and 40) for sufficiently small n might be solved directly, for example by Gaussian elimination. This has been used for two-dimensional problems (12, 21, 22). However, in three-dimensional problems, the order of the systems is usually large enough to warrant the use of iterative methods such as Jacobi's method (23): let φ^0 be a first estimate of the solution of equation 40 (for example, the potential due to the source in an infinite medium). Then one computes φ^1 from

$$\varphi^1 = \mathbf{C}^*\varphi^0 + \mathbf{g}, \tag{58}$$

φ^2 from

$$\varphi^2 = \mathbf{C}^*\varphi^1 + \mathbf{g}, \tag{59}$$

and so on for any number of iterations k. Note that we use the deflated matrix, $\mathbf{C}^*$. If the procedure converges,[4] then for sufficiently large k the vectors φ^k and φ^{k-1} are

[4] This iterative convergence should not be confused with convergence of the discrete to the continuous solutions, discussed in sections I and III.

close in the sense that (for example) the Euclidean norm of the displacement vector

$$E(k, k-1) = [\sum_{i=1}^{n} (\varphi_i^k - \varphi_i^{k-1})^2]^{1/2} \tag{60}$$

can be made as small as desired by choosing k sufficiently large.

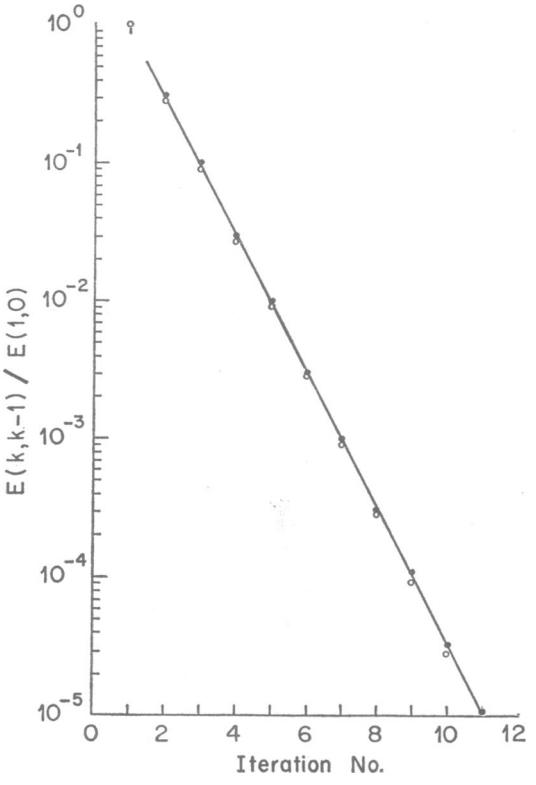

FIGURE 1 Iterative convergence for a single-sphere geometry. The solid circles are for the centric dipole and the closed circles for the displaced dipole. The convergence norm has been normalized to unity for iteration 1. The line drawn through the points has a slope of 0.31, confirming a spectral radius less than 0.5. Note that the convergence is independent of the dipole location.

Unfortunately, convergence of iterative schemes is not automatic. The condition that the procedure converge involves the "spectral radius" ρ, the largest of the magnitudes of the eigenvalues of the matrix. If $\rho(K) < 1$, the iterative procedure

$$\mathbf{q}^k = \mathbf{K}\mathbf{q}^{k-1} + \mathbf{h}, \qquad k = 1, 2, \cdots \tag{61}$$

converges for any initial estimate $\mathbf{q}^0$. If $\rho(\mathbf{K}) \geq 1$, the procedure will almost always fail to converge. It can be shown (17) that in the convex case, apart from the simple unit eigenvalue, all the other eigenvalues of both $\mathbf{B}$ and $\hat{\mathbf{B}}$ are strictly less than 1 in magnitude so that $\rho(\hat{\mathbf{C}}) < 1$. Our numerical experience and our knowledge of the continuous problem (p. 310 of reference 13) would lead us to expect that this is always the case. We have never failed to have convergence even for the most highly

convoluted multi-interface problems (see section VI). On the other hand, if the crude "centroid rule" is used, one will frequently encounter problems in which both $\rho(\hat{B}_c) > 1$ and $\rho(\hat{C}_c) > 1$ (see Table VI). Several workers have met this problem in practice.

TABLE I

ITERATIVE CONVERGENCE OF DOUBLE SPHERE WITH AND WITHOUT DEFLATION

Double sphere, 2 × 160 triangles. Radii: 1.0, 2.9. Dipole: 1.1628. Conductivity ratio: 10:1:0. First estimate: source potential only (all cases). Rule for b_{ij} : 1 solid angle.

Iteration No.	No deflation	Single deflation	Double deflation
1	18.3268	16.0800	19.6767
3	8.0636	6.0193	2.9240
5	5.2775	3.9332	0.4806
7	3.4827	2.6329	0.0879
9	2.2821	1.7625	0.0159
11	1.4799	1.1799	0.0029
13	0.9458	0.7899	0.0005
15	0.5931	0.5288	0.0001
17	0.3663	0.3540	0.000018
19	0.2318	0.2370	0.0000053
21	0.1706	0.1586	0.0000023
23	0.1605	0.1062	0.0000014
25	0.1714	0.0711	*
27	0.1855	0.0476	
29	0.1974	0.0319	
31	0.2062	0.0213	
33	0.2125	0.0142	
35	0.2168	0.0095	
37	0.2197	0.0064	
39	0.2216	0.0043	
41	0.2229	0.0029	
43	0.2238	0.0019	
45	0.2243	0.0013	
47	0.2246	0.00086	
49	0.2248	0.00058	

* Limit of computer precision.

The above remarks on iterative convergence or divergence are a special case of the theorem that the asymptotic rate of iterative convergence is more rapid the smaller the spectral radius (23). Under the convexity assumption for the single-interface problem it can be shown (17) that

$$\rho(\hat{\mathbf{C}}) \leq 1 - \hat{m}n \tag{62}$$

where

$$\hat{m} = \min_{i \neq j} (b_{ij}) \tag{63}$$

and that as a consequence for a properly discretized sphere

$$\rho(\hat{\mathbf{C}}) \leq \tfrac{1}{2} \tag{64}$$

so that we have extremely rapid rates of convergence. Fig. 1 shows the results of a calculation on a single sphere. The solid line has slope 0.31, so that equation (64) is confirmed. This figure also illustrates the well-known property (23) that the asymptotic rate of convergence is independent of the dipole location.

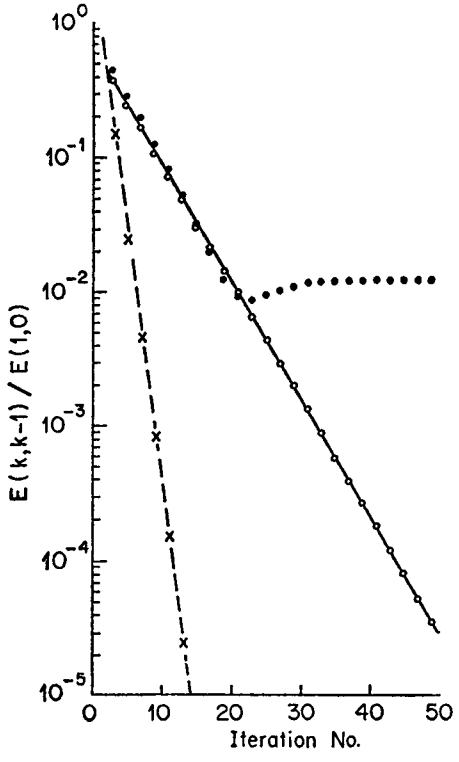

FIGURE 2 Graph of data in Table I, showing iterative behavior for double-sphere geometry. The convergence norm has been normalized to unity for iteration 1. The solid circles show the iterative behavior with no deflation, the open circles with a single deflation, and the crosses with double deflation. The solid line is the theoretical behavior for single deflation, but the dashed line has no theoretical significance.

Deflation can be used as a powerful tool to improve the iterative convergence rate, and for multiple-interface problems several deflations are desirable (18). Table I and Fig. 2 show the convergence for double-sphere geometry using zero, one, and two deflations. Without deflation, the difference between successive iterations becomes constant asymptotically (see discussion in section VI) since $\mathbf{x}^*\mathbf{g} \neq 0$ in equations 28 and 21 *a*. With single deflation the procedure converges at the theoretical rate (18) indicated by the solid line on Fig. 2. The rate of convergence improves dramatically when the second deflation is introduced, and to reduce $E(k, k-1)$ to 0.01% of its initial value takes only 12 iterations, in contrast to 44 iterations with only one deflation.

V. NUMERICAL SOLUTIONS FOR SIMPLE GEOMETRIES

For a number of simple geometries the approximate numerical solutions obtained by the methods of previous sections may be compared to exact analytical solutions. Thus, we may validate our procedures and make an explicit check on the discretization error bounds developed in section III.

Consider the following geometry: two concentric spheres of different conductivity with a source dipole displaced off-center in the direction of the dipole axis. The potentials are easily obtained analytically, as an expansion in spherical harmonics (11). The case of single spheres or centric dipoles may be regarded as special cases of the above geometry.

TABLE II

COMPARISON WITH EXACT POTENTIALS OF POTENTIALS OBTAINED NUMERICALLY

Table entry is potential in units of 10^9 v. Sphere, 704 triangles, divided equal altitudes. Radius: 1.0. Displaced dipole: 0.5.

	Centric dipole			Displaced dipole		
Latitude on sphere	Centroid	Exact	1Ω	Centroid	Exact	1Ω
+6	25.01	24.72	24.59	56.83	55.11	54.68
+5	18.78	20.22	20.30	19.26	20.98	21.41
+4	14.81	15.73	15.82	6.77	7.19	7.39
+3	10.62	11.24	11.31	0.12	0.01	0.11
+2	6.38	6.74	6.79	−3.88	−4.28	−4.23
+1	2.13	2.25	2.27	−6.48	−7.09	−7.07
−1	−2.13	−2.25	−2.27	−8.28	−9.05	−9.04
−2	−6.38	−6.74	−6.79	−9.60	−10.47	−10.47
−3	−10.62	−11.24	−11.31	−10.57	−11.55	−11.55
−4	−14.81	−15.73	−15.82	−11.30	−12.39	−12.39
−5	−18.78	−20.22	−20.30	−11.78	−13.05	−13.05
−6	−25.01	−24.72	−24.59	−13.21	−13.59	−13.52

We have made an extensive series of calculations in which we computed numerically the potential distribution both via charge (equation 34) and directly (equation 40). These were carried out for single and double spheres, approximating the spheres by different numbers of triangles. These numerical results have the form of the *average* potential over a triangle, so before making the comparison we took the weighted average of adjacent base-up and base-down triangles. This then is the average potential over a plane quadrilateral, $\varphi_{\text{numerical}}$. Analytically it is easy to average the spherical-harmonic expansion over a spherical quadrilateral to obtain $\varphi_{\text{analytic}}$. These two quantities may legitimately be compared (see section III). Our objectives were to demonstrate the convergence of the discrete to the continuous problem and to compare the quality of solutions obtained via the charge equation with those directly from the potential equation.

TABLE III

VALUES OF χ_φ FOR POTENTIALS OBTAINED VIA CHARGE EQUATIONS FOR SINGLE SPHERES

Table entry is χ_φ in units of 10^9 v. Sphere divided by equal angles subtended. Radius: 1.0. Displaced dipole: 0.5.

Number of triangles	δ	Centric dipole		Displaced dipole	
		Centroid	1Ω	Centroid	1Ω
160	0.632	0.736	0.395	2.58	0.827
352	0.464	0.410	0.636	1.13	1.18
704	0.324	0.718	0.190	3.73	0.369
1472	0.235	0.352	0.227	1.751	0.485

TABLE IV

VALUES OF χ_φ FOR POTENTIALS OBTAINED DIRECTLY FROM POTENTIAL EQUATION FOR SINGLE SPHERES

Table entry is χ_φ in units of 10^9 v. Sphere divided by equal altitudes. Radius: 1.0. Displaced dipole: 0.5.

Number of triangles	δ	Centric dipole		Displaced dipole	
		Centroid	1Ω	Centroid	1Ω
160	0.817	1.374	0.3882	1.268	0.6522
352	0.577	1.506	0.4538	1.503	0.6543
704	0.577	1.441	0.1251	1.725	0.4255
1472	0.408	1.220	0.1106	1.608	0.3338
1856	0.365	1.126	0.1148	1.528	0.2323

TABLE V

VALUES OF χ_φ FOR POTENTIALS OBTAINED DIRECTLY FROM POTENTIAL EQUATION FOR DOUBLE SPHERES

Table entry is χ_φ in units of 10^9 v. Multiple deflation used. Spheres divided by equal altitudes. Radii: 1.0, 2.9. Displaced dipole: 1.1628. Conductivity ratio: 10:1:0.

Number of triangles	Centric dipole		Displaced dipole	
	Centroid	1Ω	Centroid	1Ω
2 × 160	0.775	0.566	0.593	0.466
2 × 352	0.862	0.413	0.574	0.516
2 × 704	0.889	0.395	0.535	0.543

In Table II the analytic and numerical potentials are shown for the case of a single sphere, represented for the numerical calculation by 704 triangles. This illustrates the importance of careful evaluation of the b_{ij}, since the numerical results using "one solid angle" are clearly more accurate than those using "centroid rule."

Table III shows the results for potential obtained via the charge equation for

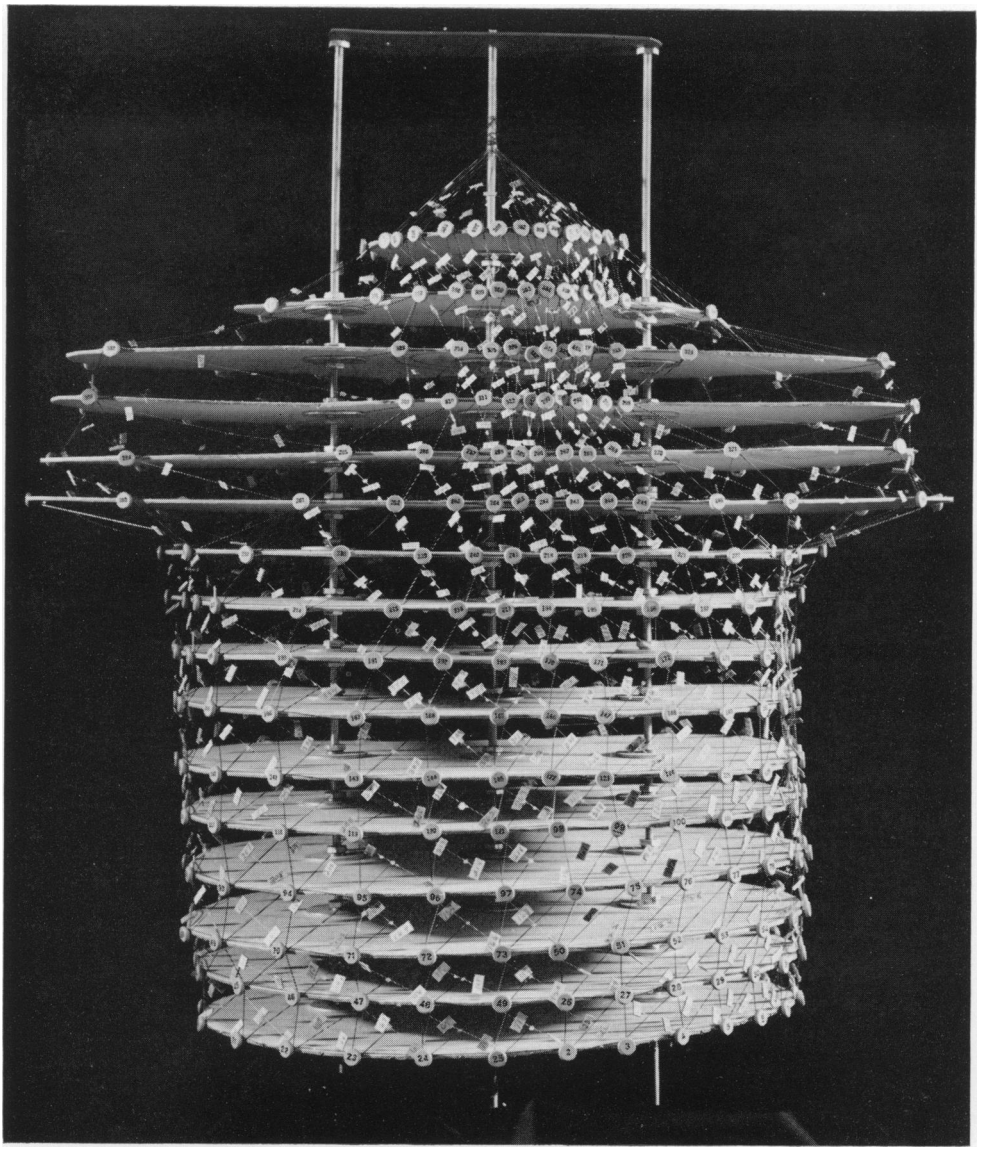

FIGURE 3 Photograph of a model showing the geometry used for the realistic torso surface. The triangularization is indicated by threads on the model, and the numbers identify the triangles and vertices.

single spheres. The potential error norm

$$\chi_\varphi = \max | \varphi_{\text{numerical}} - \varphi_{\text{analytic}} | \tag{65}$$

is the entry in the table. Tables IV and V show the results for potentials obtained

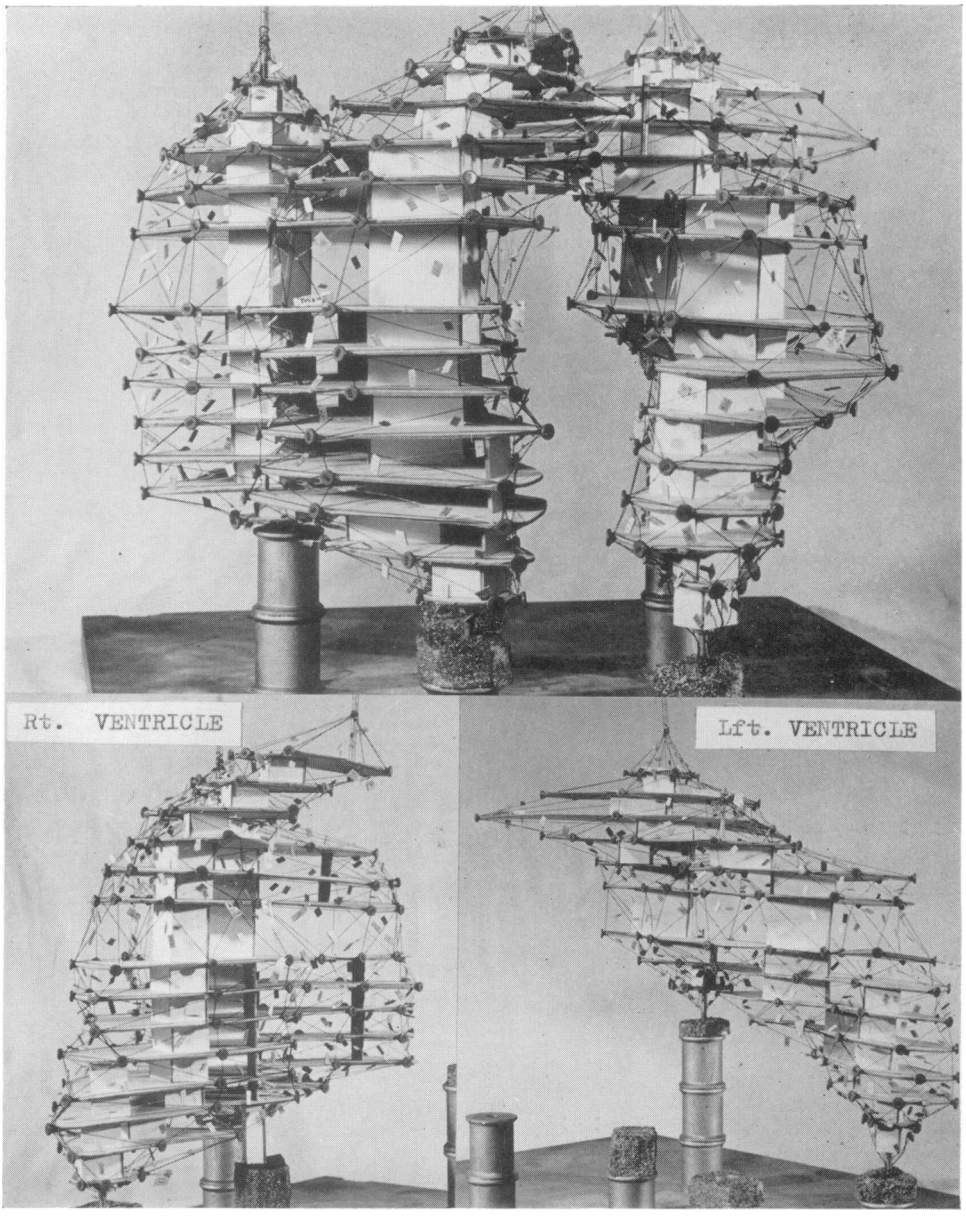

FIGURE 4 Photograph of a model showing the geometry used for the realistic intraventricular blood masses. The triangularization is indicated by threads on the model, and the numbers identify the triangles and vertices.

TABLE VI

ITERATIVE CONVERGENCE OF LEFT VENTRICLE CALCULATIONS

Method: Potential directly. First estimate: Source potential only (all cases).

	"Centroid rule"		"One solid angle rule"	
Iteration No.	No deflation	With deflation	No deflation	With deflation
1	115329	91593	124655	99566
3	80199	59176	94112	55516
5	172196	276902	84244	36511
7	1168843	1990828	80054	24841
9	8477420	5403509	78242	17184
11	61980863	106371551	77479	12044
13	larger	larger	77180	8547
15			77082	6142
17			77067	4471
19			77084	3299
21			77110	2467
23			77136	1870
25			77158	1435
27			77176	1115
29			77190	875
31			77199	693
33			77205	554
35			77209	445
37			77210	359
39			77209	292
41			77207	237
43			77204	194
45			77200	158
47			77195	129
49			77190	106

directly from the potential equation for single and double spheres. In all cases the source was a unit-strength electrostatic dipole, i.e., 1 coulomb-meter. This is a very large dipole and produces potentials of the order of 10^{11} v. Of course, the potentials simply scale for other dipole strengths.

A study of these tables reveals that it generally appears preferable to compute potential directly using "one solid angle" rather than via charge, consistent with the results outlined in section III. There is consistent evidence that the "one solid angle" is to be preferred, even in these simple analytic cases, to the "centroid rule;" indeed, there is no evidence of convergence of the latter in Table IV as the number of triangles increases, whereas eventual convergence is ensured for the former (see section III).

We remarked in section III that convergence of the discrete towards the continu-

ous solutions for the "one solid angle" rule need not be monotonic. This is confirmed by the results in Tables II–IV.

We noted in section IV that the accuracy of evaluation of matrix elements b_{ij} could affect the iterative convergence even in simple analytic geometries. This has been confirmed during our calculations with triple sphere geometry, since the iterations diverged using "centroid rule" but converged using "one solid angle." This

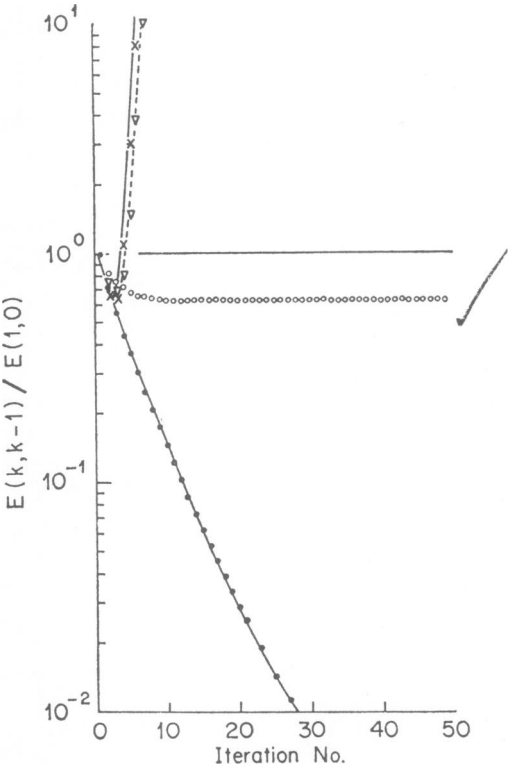

FIGURE 5 Iterative convergence for the left ventricle. The convergence norm has been normalized to unity for iteration 1. The crosses and triangles show the divergent behavior using the "centroid rule." The open and closed circles show the convergent behavior using "one solid angle." The open circles are for the calculation without using deflation. The closed circles are for the calculation using deflation.

point is far more manifest when one considers realistic torso geometries, as discussed in the next section.

Another comparison between the direct method of computing potential and that of computing potential via charge is discussed at the end of section VII, in the context of an "inverse" problem

VI. NUMERICAL SOLUTIONS FOR REALISTIC TORSO GEOMETRIES

We obtained our torso geometry data from the cross-section anatomy of reference 6. Dr. L. L. Hefner, of the University of Alabama Medical Center, has coordinated

these data not only for the thoracic surface, but also for the endocardiac and pulmonary surfaces.

These various surfaces were triangularized, and the coordinates of the vertices form the representation of the surface for computing purposes. Figs. 3 and 4 show photographs of models of the torso surface and ventricular blood masses, respectively.

The source dipoles were located at various points in the myocardium. Although we have restricted our computations to dipole sources, there is no difficulty in extending them to any even multipolar source

As another example of the importance of careful evaluation of the matrix elements b_{ij}, Table VI and Fig. 5 show results for the single-interface problem of the left ventricle alone. If the matrix elements are approximated by the "centroid rule,"

TABLE VII

EFFECT ON POTENTIALS OF CONSTANT DIFFERENCE BETWEEN ITERATIONS WITH NO DEFLATIONS*

Table entry is potential in units of 10^{14} v. Results shown only for six of the 364 elements.

Surface element No.	No deflation			With deflation	
	Iteration No.			Iteration No.	
	9	49	Subtract 1.966	9	49
1	0.197	1.843	−0.123	−0.153	−0.123
2	0.175	1.820	−0.146	−0.175	−0.146
3	0.173	1.819	−0.147	−0.176	−0.147
4	0.203	1.776	−0.190	−0.146	−0.189
5	0.205	1.777	−0.189	−0.145	−0.188
6	0.216	1.864	−0.102	−0.134	−0.102

* Same case as Table VI.

the iterative procedure initially converges, for three iterations, but then diverges drastically with or without deflation. If the "one solid angle" approximation is used without deflation, the differences between successive iterations become almost constant (not zero) after a few iterations. The potentials then grow, as shown in Table VII. Theoretically at each iteration a scalar multiple of **e** is added to φ and can be subtracted out later (column 4 of Table VII). However, this is precisely equivalent to deflation, which is more simply performed once on the coefficient matrix **B**, instead of on every dipole at every iteration. Furthermore, the latter does not carry over to the multi-interface problem where the situation is considerably more complex (18). There is also the additional danger that the background "noise," which accumulates linearly with each iteration, may, if sufficiently severe, dominate the "signal," with resultant loss of accuracy

Calculations with varying degrees of complexity have been made, ranging from

the trivial "infinite homogeneous medium" case, where the effects of all interfaces are neglected, to the most complete case where torso, both ventricles, and both lungs are included and multiple deflation must be employed to insure rapid convergence. The direct results of the calculation are in the form of potentials averaged over each element. For the purpose of presentation, these potentials are mapped on a cylinder which is then opened out. Some results are shown in Fig. 6.

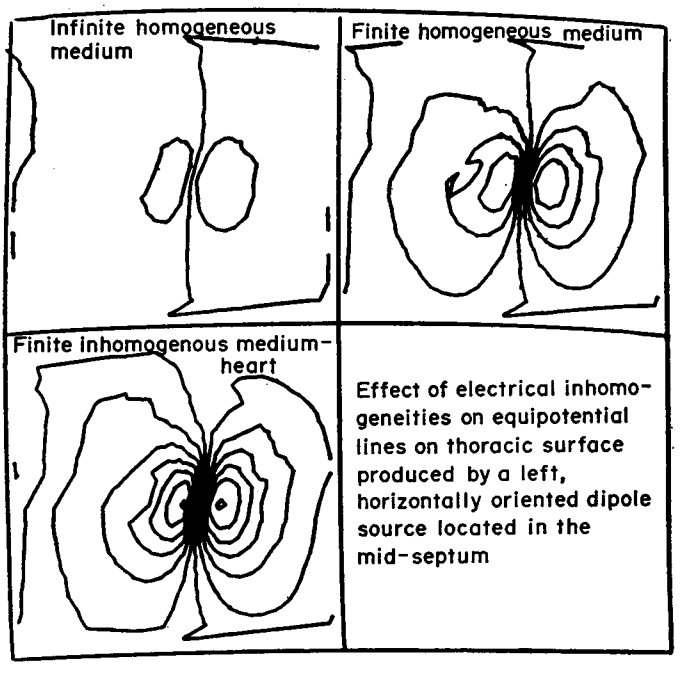

FIGURE 6 Surface potential maps computed for three modeling assumptions. Top left: infinite homogeneous medium, all surfaces ignored; top right: finite homogeneous medium, torso surface only included; bottom left: finite inhomogeneous medium, torso surface plus intraventricular blood masses. The source was a unit-strength dipole located in the septum, pointing horizontally from right to left. The potentials at the torso surface were mapped on a cylinder which was cut at the back and opened out.

VII. SIMPLE CASES OF THE INVERSE PROBLEM

In previous sections we have outlined how to obtain surface potentials for specified internal sources, e.g., a unit-strength dipole with some given position and orientation. This may be called "the forward problem." Clinically, the more interesting problem is the "inverse problem" (given the surface potentials, determine the sources). This is the subject of a forthcoming paper (15), but at this point we consider briefly a particularly simple example of the inverse problem: given a set of surface potentials, what single dipole best reproduces them? This is, of course, an extension of the "vectorcardiogram." Our motivation for including it in a paper

otherwise limited to aspects of the forward problem is to show that the labor of including in the theory the effects of internal thoracic inhomogeneities has been no mere academic exercise. We shall show that the modeling assumptions greatly affect the results.

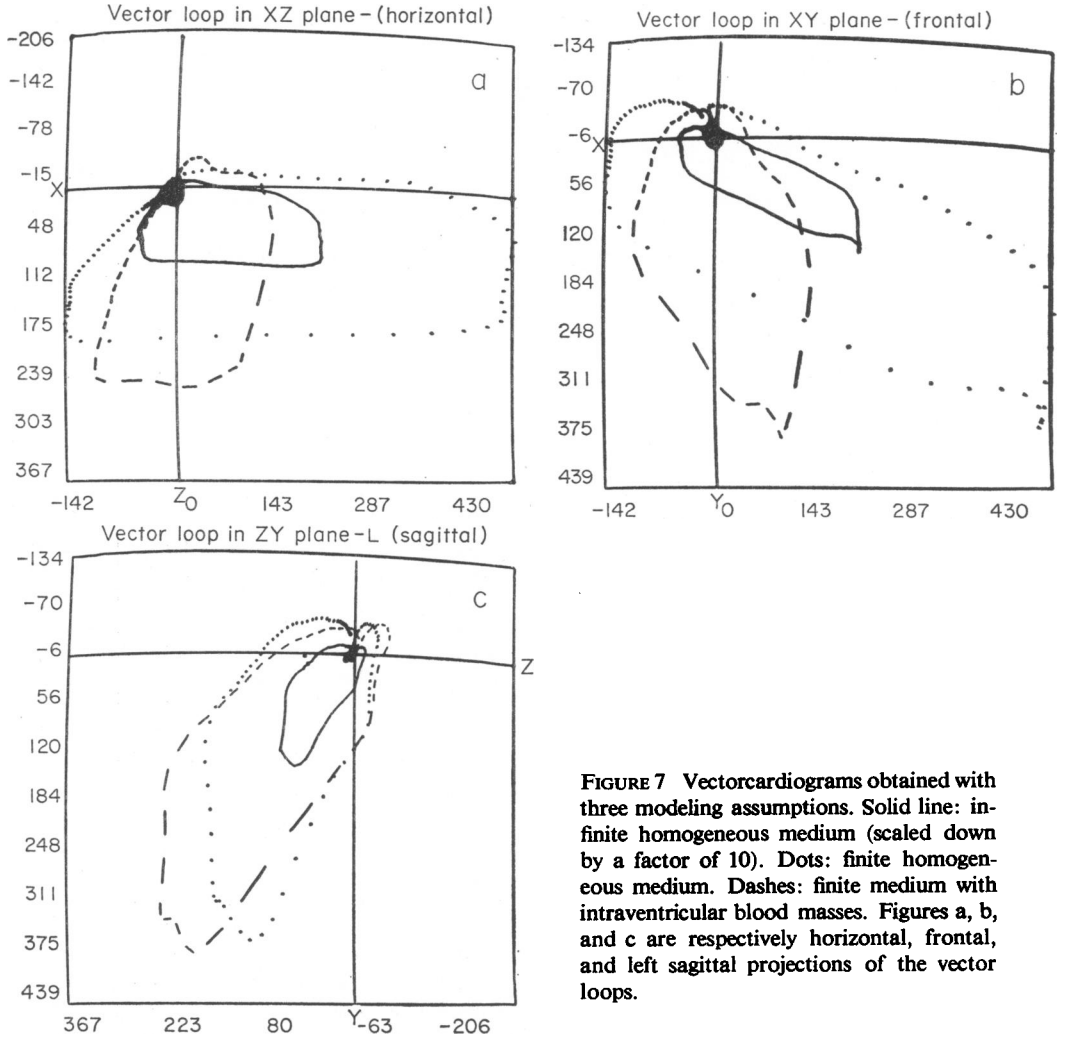

FIGURE 7 Vectorcardiograms obtained with three modeling assumptions. Solid line: infinite homogeneous medium (scaled down by a factor of 10). Dots: finite homogeneous medium. Dashes: finite medium with intraventricular blood masses. Figures a, b, and c are respectively horizontal, frontal, and left sagittal projections of the vector loops.

First, surface potentials were calculated for three unit-strength, orthogonal dipoles located in the septum. The calculations were made with three modeling assumptions: (*a*) all surfaces ignored (infinite homogeneous medium), (*b*) only thoracic surface included (finite homogeneous medium), (*c*) thoracic surface plus ventricular blood masses included.

The inverse problem was then run for each of the three cases by taking measured surface potentials[5] and making a "least squares" fit to determine the best combination of the three dipoles at each point in time. These three dipole strengths are the

TABLE VIII

APPLICATION OF THE GABOR AND NELSON TECHNIQUE

No.	Name	Original	Via charge	Direct
	8(a): Strengths			
1	Sup. ante. septum	1.0000	0.9936	0.9934
2	Mid-Rt. vent.	1.0000	0.9990	1.0044
3	Mid-Left vent.	1.0000	0.9961	0.9908
4	Inf. post. septum	1.0000	0.9933	0.9898
5	Low ante-lat. left vent.	1.0000	0.9923	0.9851
6	Ant. mid-septum	1.0000	0.9898	0.9888
7	Ant. rt. vent.	1.0000	0.9942	0.9917
8	Mid ante. left vent.	1.0000	0.9876	0.9886
9	Low post. left vent.	1.0000	0.9952	0.9909

Dipole No.	*x*			*y*			*z*		
	Orig.	Chg.	Dir.	Orig.	Chg.	Dir.	Orig.	Chg.	Dir.
				8(b): Locations					
1	0.0628	0.0634	0.0626	0.0207	0.0200	0.0197	0.2463	0.2459	0.2467
2	0.0940	0.0937	0.0940	0.0110	0.0127	0.0111	0.2320	0.2326	0.2329
3	0.0450	0.0454	0.0440	0.0450	0.0440	0.0439	0.2170	0.2168	0.2177
4	0.0450	0.0447	0.0443	0.0050	0.0055	0.0061	0.2220	0.2226	0.2228
5	0.0701	0.0707	0.0704	0.0653	0.0635	0.0634	0.2186	0.2172	0.2188
6	0.0800	0.0803	0.0801	0.0350	0.0345	0.0346	0.2170	0.2178	0.2187
7	0.0950	0.0937	0.0949	0.0400	0.0385	0.0384	0.2080	0.2088	0.2093
8	0.0666	0.0672	0.0664	0.0604	0.0598	0.0603	0.2426	0.2426	0.2430
9	0.0330	0.0348	0.0314	0.0260	0.0255	0.0253	0.2170	0.2162	0.2177
				8(c): Dipole Components					
1	0.6464	0.6443	0.6458	−0.6320	−0.6254	−0.6242	0.4271	0.4253	0.4243
2	0.9745	0.9751	0.9796	−0.2220	−0.2146	−0.2208	0.0259	0.0337	0.0231
3	−0.7071	−0.7035	−0.7021	0.0	−0.0025	−0.0043	−0.7071	−0.7052	−0.6991
4	−0.9042	−0.8999	−0.8969	−0.3014	−0.2957	−0.2938	−0.3014	−0.2989	−0.2982
5	−0.0970	−0.0970	−0.1017	0.6209	0.6096	0.6049	−0.7770	−0.7769	−0.7708
6	0.5739	0.5715	0.5731	−0.8200	−0.8081	−0.8058	0.0	0.0010	−0.0019
7	0.8660	0.8596	0.8562	0.0	0.0048	0.0008	−0.5000	−0.4995	0.5004
8	0.1118	0.1144	0.1092	0.9540	0.9412	0.9440	0.2778	0.2765	0.2726
9	−0.3740	−0.3715	−0.3730	0.0353	0.0324	0.0326	−0.9260	−0.9226	−0.9174

orthogonal components of the single dipole best representing the cardiac generator at that time interval, i.e., we have the data for a vectorcardiogram. The results are shown in Fig. 7. It can be seen that the vectorcardiograms are quite sensitive to the

[5] The authors are indebted to Dr. John Holt for providing these measurements.

modeling assumptions. The difference between infinite and finite homogeneous media is approximately a scale factor,[6] and thus unimportant. However, the inclusion of the ventricular blood [case (*c*)] produces quite drastic changes in the vectorcardiogram.

Gabor and Nelson (7) give an expression for the location, strength, and direction of the resultant dipole, given the complete distribution of potential over the surface of a homogeneous conductor. Their result can be used to provide a further validation of our methods.

Calculations were made for unit strength dipoles placed at various myocardial locations within the homogeneous conductor of realistic torso shape. The forward problem was solved computing the surface potential distribution both via charge and directly. The Gabor and Nelson technique was then applied. Since we started with pure dipole sources, theoretically we should be able to recover precisely the originally assumed location, strength, and direction of these sources. The results are shown in Table VIII, and it can be seen, on the one hand, that we recover the source specifications surprisingly accurately, and on the other hand, that we attain this accuracy with either method of computation. In the context of the Gabor and Nelson application it would seem that either method is satisfactory; this does not necessarily extend to other applications. For example, when inhomogeneities are taken into consideration, the methods yield potential distributions which sometimes differ significantly.

VIII. SUMMARY

Discrete analogues have been derived for the singular integral equations obtained when electromagnetic theory is applied to electrocardiology. It has been demonstrated that the analogues may be solved iteratively in a stable and convergent manner, provided that careful numerical methods are used. The validity of the methods has been established for geometries sufficiently simple that exact analytical solutions exist, with which the numerical solutions may be compared. The methods have also been applied to the "forward problem" with realistic thoracic geometries, including the major internal inhomogeneities (lungs and cardiac blood masses). Finally, a simple example of the "inverse problem" has demonstrated the importance of the internal inhomogeneities.

The authors gratefully acknowledge the contribution of Messrs. R. H. Crane, D. E. Richards, J. Allen, and the many other programmers and assistants who worked long hours programming and running the calculations reported in this paper. The continuing cooperation between this Center and many persons at the University of Alabama Medical Center has been the source of much help and stimulation to the authors. In the context of this paper we particularly want to thank Lloyd L. Hefner, M.D. for providing the data on the realistic geometry of torso, lungs, and ventricular blood masses, and John H. Holt, M.D. for supplying in vivo surface potentials. The authors would also like to

[6] If the thoracic surface were a sphere, this would be precisely so.

thank Professor Leo Horan and Richard Martin of the University of Tennessee Department of Medicine for drawing our attention to the Gabor and Nelson technique used in section VII.

Received for publication 16 January 1967.

APPENDIX I

EXACT ANALYTIC EXPRESSION FOR THE SOLID ANGLE SUBTENDED BY A TRIANGLE AT A POINT

If $\mathbf{r}_1$, $\mathbf{r}_2$, $\mathbf{r}_3$ are vectors from the point to the three vertices of the triangle, then a quantity α may be defined by

$$\alpha = \tan^{-1} \frac{|(\mathbf{r}_3 \times \mathbf{r}_1) \times (\mathbf{r}_1 \times \mathbf{r}_2)|}{-(\mathbf{r}_3 \times \mathbf{r}_1) \cdot (\mathbf{r}_1 \times \mathbf{r}_2)}$$

and quantities β and γ defined by cyclic permutation of the indices. A vector $\mathbf{c}$ may be drawn from the point to the centroid of the triangle and a unit vector $\mathbf{n}$ drawn in the outward normal direction to the triangle. Then the solid angle is given exactly by

$$\Omega = (\alpha + \beta + \gamma - \pi)(\mathbf{c} \cdot \mathbf{n})/|\mathbf{c} \cdot \mathbf{n}|.$$

Although this result is theoretically exact, care has to be taken with the numerical precision. An appropriate subroutine is available from the authors.

REFERENCES

1. BARNARD, A. C. L., I. M. DUCK, and M. S. LYNN. 1967. *Biophys. J.* **7**:443.
2. BARR, R. C., T. C. PILKINGTON, J. P. BOINEAU, and M. S. SPACH. 1966. *IEEE (Inst. Elec. Electron Engrs.) Trans. Bio-Med. Eng.* **13**:88.
3. BERRY, P. M. 1957. *Ann. N. Y. Acad. Sci.* **67**:1003.
4. BODEWIG, E. 1956. Matrix Calculus. North Holland Publishing Co., Amsterdam, The Netherlands.
5. COURANT, R., and D. HILBERT. 1962. Methods of Mathematical Physics. John Wiley & Sons, Inc., New York, **1**.
6. EYCLESHYMER, A. C., and D. M. SHOEMAKER. 1911. A Cross-Section Anatomy. Appleton-Century & Appleton-Century-Crofts, New York.
7. GABOR, D., and C. V. NELSON. 1954. *J. Appl. Phys.* **25**:413.
8. GELERNTER, H. L., and J. SWIHART. 1964. *Biophys. J.* **4**:285.
9. GELERNTER, H. L., and J. SWIHART. 1965. Electrophysiology of the Heart. B. Taccardi and G. Marchetti, editors. Pergamon Press, Inc., New York. 229.
10. GELERNTER, H. L., and J. SWIHART. 1965. Computer Solution of an Extended Form of the Neumann Problem with Particular Applications in Electrophysiology. Proceedings of the 3rd All-Union Conference on Automatic Control and Technical Cybernetics. Odessa, U. S. S. R. 42.
11. JACKSON, J. D. 1962. Classical Electrodynamics. John Wiley & Sons, Inc., New York.
12. JASWON, M. A. 1963. *Proc. Royal Soc. (London), Ser. A.* **275**:23.
13. KELLOGG, O. D. 1929. Foundations of Potential Theory. Frederick Ungar Publishing Co., Inc., New York.
14. KIRK, W. L., JR., R. H. SELVESTER, and C. COLLIER. 1966. Estimation of the Activation Front of the Heart from Body Surface ECG Measurements. Proceedings of the 19th Annual Conference on Engineering in Medicine and Biology. San Francisco. 192.
15. LYNN, M. S., J. H. HOLT, JR., W. H. LYNE, J. EVANS, L. L. HEFNER, and L. T. SHEFFIELD. 1967.

A Multiple Dipole Electrocardiogram. Southern Society for Clinical Investigation, 21st Annual Meeting, New Orleans. 56.
16. LYNN, M. S., and W. P. TIMLAKE. 1966. On the Numerical Solution of the Singular Integral Equations and Applications to Electrocardiology. SIAM National Meeting, University of Iowa.
17. LYNN, M. S., and W. P. TIMLAKE. 1966. On the Numerical Solution of the Singular Integral Equations of Potential Theory. Numerische Mathematik. In press.
18. LYNN, M. S., and W. P. TIMLAKE. 1967. The Use of Multiple Deflations in the Numerical Solution of Singular Systems of Equations, with Applications to Potential Theory. *SIAM Journal Ser. B.* In press.
19. PLONSEY, R. 1966. Field Techniques in Electrocardiography. Proceedings of the 19th Annual Conference on Engineering in Medicine and Biology. San Francisco. 251.
20. ROGERS, C. L., T. C. PILKINGTON, J. P. BOINEAU, and M. S. SPACH. 1966. On the Inverse Problem of Electrocardiography. Proceedings of the 19th Annual Conference on Engineering in Medicine and Biology. San Francisco. 135.
21. SYMM, G. T. *Proc. Roy. Soc. (London), Ser. A.* **275**:33.
22. SYMM, G. T. 1964. Integral Equation Methods in Elasticity and Potential Theory. Doctoral Dissertation. University of London.
23. VARGA, R. S. 1962. Matrix Iterative Analysis. Prentice-Hall, Inc., Englewood Cliffs, N. J.
24. WILSON, F. N., and R. H. BAYLEY. 1950. *Circulation.* **1**:84.